Impact of ATLAS constraints on effective dark matter-standard model interactions with spin-one mediators

Fabiola Fortuna and Pablo Roig
Centro de Investigación y de Estudios Avanzados, Apartado Postal 14-740, 07000, Ciudad de México, Mexico

(Received 1 November 2022; accepted 15 March 2023; published 6 April 2023)

We complement a previous work [Fabiola Fortuna *et al.*, Effective field theory analysis of dark matter-standard model interactions with spin one mediators, J. High Energy Phys. 02 (2021) 223.] using an effective field theory framework of dark matter and standard model interactions, with spin-one mediators, exploring a wider dark matter mass range, up to 6.4 TeV. We again use bounds from different experiments: relic density, direct detection experiments, and indirect detection limits from the search of gamma-ray emissions and positron fluxes. Additionally, in this paper we add collider constraints by the ATLAS Collaboration in the monojet analysis. Moreover, here we tested our previous results in the light of the aforementioned ATLAS data, which turns out to be the most restrictive for light dark matter masses (as expected), $m_{\mathrm{DM}} < M_Z/2$. We obtain a larger range of solutions for the operators of dimension 5, OP1 and OP4, where masses above 43 GeV and 30 GeV [except for the Z-resonance region, $\sim(M_Z \pm \Gamma_Z)/2$], respectively, are allowed. In contrast, the operator of dimension 6, OP3, has viable solutions for masses $\gtrsim$190 GeV. For the combination of OP1 and OP3 we obtain solutions (for masses larger than 140 GeV or 325 GeV) that depend on the relative sign between the operators.

DOI: 10.1103/PhysRevD.107.075003

I. INTRODUCTION

Understanding the fundamental nature of Dark Matter (DM) is one of the most compelling problems in particle physics and cosmology, yet despite years of searching, the identity of DM remains a mystery. A favored paradigm for the particle nature of dark matter is that of weakly interacting massive particles (WIMPs) [1–3]. In this scenario the DM interactions with the Standard Model (SM) are sufficiently weak to meet the constraints of direct- [4–10] and indirect-detection experiments [11–21], but strong enough to generate the relic abundance inferred from measurements of the cosmic microwave background radiation [22]. In absence of any direct DM signal, the generality of the effective field theory (EFT) approach may be advantageous [23–29], as it only uses the known SM symmetries and degrees of freedom, assuming that the typical energy of all relevant processes lies below the mediator mass. We will follow such an approach by using an effective Lagrangian to parametrize the interactions of the dark sector with the SM, and determine the restrictions imposed by the experimental/observational constraints. The Higgs portal (see Ref. [30] and references therein) and neutrino portal cases [31–47] have received considerably more attention than the case of spin-one mediators, so we will focus on the latter both in the Proca or antisymmetric-tensor representations.

Here we will continue exploring the phenomenological consequences of the EFT scenario developed in Ref. [48] for the interactions between SM and DM particles with heavy mediators. We have already studied the low-energy region, with DM masses under $m_Z/2$ in Ref. [49]. In that analysis, we found solutions complying with the constraints imposed: Z invisible decay width [50], relic density [50], direct detection limits from Xenon1T [51], PandaX [52], LUX [53], DarkSide-50 [54], and CRESST-III [55]. We also employed indirect-detection limits from the search of gamma-ray emissions [56] and positron fluxes [57]. In this work we extend the region of DM masses under analysis, from 50 GeV up to 6.4 TeV (slightly less than half the LHC c.m. collision energy, as our DM particles need to be pair produced, accounting for the detection jet-energy threshold). We use again the restrictions mentioned above and we add collider constraints by the ATLAS Collaboration [58]. In fact we also tested our previous results from the low-energy region against the ATLAS data and further restricted the space of solutions.

The paper is organized as follows: In Sec. II we introduce the EFT that we are using [48] and highlight the part interesting for this study and our conventions. Then in

Sec. III we analyze several observational limits; in Sec. III A we check that the observed relic abundance can be reproduced in the different cases, in Sec. III B we verify the direct detection bounds are respected, and in Secs. III C and III D we consider the indirect bounds given by dwarf spheroidal satellite galaxies and the positron flux, respectively. After that, in Sec. IV we include the collider constraints by the ATLAS Collaboration. Finally the discussion and conclusions are presented in Sec. V.

II. EFFECTIVE LAGRANGIAN

We study interactions between dark matter and standard model particles using an effective field theory approach, where we consider that the heavy mediators that generate the interaction are of spin-one. In the dark sector we can have scalars Φ, fermions Ψ, and vectors X. The mediators are weakly coupled to both sectors, dark and standard, and this information is encoded in the effective coefficients X_{eff}. We assume that the dark fields transform nontrivially under a symmetry group, $\mathcal{G}_{\mathrm{DM}}$ (that we do not need to specify), while all SM particles are singlets under this $\mathcal{G}_{\mathrm{DM}}$, which ensures the stability of the DM particle. Also, all dark fields are singlets under the SM gauge group. The consequence of interactions generated by a mediator are that our operators have the form,

$$\mathcal{O} = \mathcal{O}_{\mathrm{SM}}\mathcal{O}_{\mathrm{dark}}, \tag{1}$$

and we know that O_{dark} contains at least two fields because we have assumed that the dark fields transform nontrivially under $\mathcal{G}_{\mathrm{DM}}$. In the effective Lagrangian, each term has a factor $1/\Lambda^n$, $n = \dim(\mathcal{O})$-4, where Λ is of the order of the heavy mediator mass(es). We restricted ourselves to operators of mass dimension ≤ 6. In this work, we focus on operators with vector and antisymmetric tensor mediators because the models with scalar and fermion mediators have already been studied extensively [24,27,40,59–67].

The Lagrangian we use is conveniently separated into two parts where ψ stands for SM fermions and $B_{\mu\nu}$ is the $U(1)_Y$ field-strength tensor (universal couplings to the SM fermions are assumed):

(i) Terms involving dark fermions (Ψ),

$$\mathcal{L}^{\Psi}_{\mathrm{eff}} = \frac{\Upsilon_{\mathrm{eff}}}{\Lambda} B_{\mu\nu}\bar{\Psi}\sigma^{\mu\nu}\Psi + \frac{A^{L,R}_{\mathrm{eff}}}{\Lambda^2}\bar{\psi}\gamma_\mu\psi\bar{\Psi}\gamma^\mu P_{L,R}\Psi + \frac{\kappa^{L,R}_{\mathrm{eff}}}{\Lambda^2} B_{\mu\nu}\bar{\Psi}(\gamma^\mu \overleftrightarrow{\mathcal{D}}^\nu - \gamma^\nu \overleftrightarrow{\mathcal{D}}^\mu)P_{L,R}\Psi. \tag{2}$$

(ii) Terms involving dark bosons (X, Φ),

$$\mathcal{L}^{\Phi,X}_{\mathrm{eff}} = \frac{\zeta_{\mathrm{eff}}}{\Lambda} B_{\mu\nu}X^{\mu\nu}\Phi + \frac{\epsilon_{\mathrm{eff}}}{\Lambda^2}\bar{\psi}\gamma_\mu\psi\frac{1}{2i}\Phi^\dagger \overleftrightarrow{\mathcal{D}}^\mu\Phi. \tag{3}$$

III. OBSERVATIONAL LIMITS

We use the following notation for our operators[1]:

$$\begin{aligned}
\mathrm{OP1} &\equiv B_{\mu\nu}\bar{\Psi}\sigma^{\mu\nu}\Psi,\\
\mathrm{OP2} &\equiv \bar{\psi}\gamma^\mu\psi\bar{\Psi}\gamma_\mu P_{L,R}\Psi,\\
\mathrm{OP3} &\equiv B_{\mu\nu}\bar{\Psi}(\gamma^\mu \overleftrightarrow{\mathcal{D}}^\nu - \gamma^\nu \overleftrightarrow{\mathcal{D}}^\mu)P_{L,R}\Psi,\\
\mathrm{OP4} &\equiv B_{\mu\nu}X^{\mu\nu}\Phi,\\
\mathrm{OP5} &\equiv \frac{1}{2i}(\bar{\psi}\gamma^\mu\psi)(\Phi^\dagger \overleftrightarrow{\mathcal{D}}_\mu\Phi).
\end{aligned} \tag{4}$$

We also consider the combined contributions from dimension-5 and dimension-6 operators when they contain the same DM candidate; in such cases we adopt the following relationship between the scales Λ and operator coefficients C:

$$\Lambda_{\mathrm{dim}\,6} = \Lambda_{\mathrm{dim}\,5}, \qquad C_{\mathrm{dim}\,6} = \pm C_{\mathrm{dim}\,5}. \tag{5}$$

In most combinations, the relative sign between coefficients is irrelevant, with the exception of the combination between OP1 and OP3, where phenomenology can vary slightly depending on their relative sign.

We are using $\Lambda = 2m_{\mathrm{DM}}$ when combining operators of different dimensions.[2,3] We consider that equality is a safe limit for the convergence of the effective theory, as discussed in [64]. Also in [69], the authors use the same relationship for their calculations to be meaningful in the EFT framework. Depending on the UV completion of the theory, a possible s-channel process in the high-energy theory might break the EFT when the corresponding heavy mediator resonates. We have checked that our results change insignificantly, moving slightly away from the previous equality ($\Lambda \gtrsim 2m_{\mathrm{DM}}$). Hereafter, we will be expressing constraints on ratios of effective couplings over $\Lambda^{(2)}$ as bounds on the couplings by using $\Lambda = 2m_{\mathrm{DM}}$, for

[1]We note the recent study of Ref. [68] using OP4, in the context of feebly-coupled vector-boson DM.

[2]Although all operators that we consider in this work can, in principle, be generated at tree level by spin-one mediators neutral under both SM and DM gauge groups [48], a caveat is in order. If the dimension-5 operators are generated at loop level, the ratio m_{DM}/Λ could be a few orders of magnitude smaller. This would depend on the hierarchy between m_{DM} and m_{loop} (the mass of the inner particle in the loop, not necessarily the mediator or the DM particle), and that is completely model dependent.

[3]A comment on the operator coefficients is pertinent; depending on the working assumptions (neutral or charged mediators under SM and DM gauge groups, mediators' spin, etc.) a given operator can be generated at tree level or first appears at one loop (see Sec. 2.1. of [48]). If the underlying physics is weakly coupled, the coefficient is suppressed by $\sim 1/(16\pi^2)$, which may require an unnaturally large dimensionless coupling value, that (on the contrary) would be expected if the underlying physics is strongly coupled.

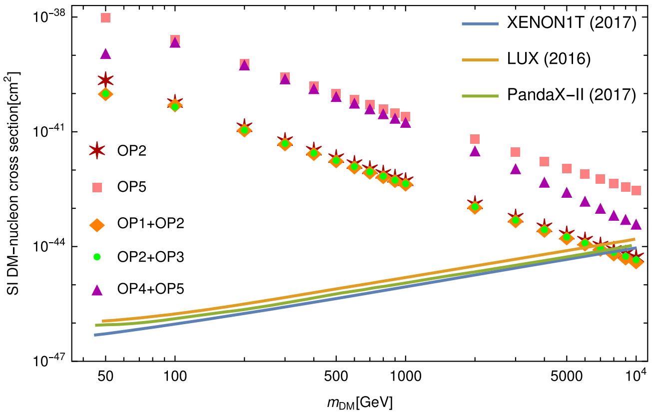

FIG. 1. WIMP cross sections (normalized to a single nucleon) for spin-independent coupling versus mass. The notation in this figure is defined in Eq. (4). When we combine operators with the same DM candidate, we use $\Lambda = 2m_{\rm DM}$. Operators not shown here have cross sections many orders of magnitude below the current limits.

given DM masses. When combining operators, sticking to the case $\Lambda = 2m_{\rm DM}$ maximizes the impact of higher-dimensional operators, through their interference with the leading ones, while keeping the convergence of the EFT. Of course, solutions can be found for $\Lambda > 2m_{\rm DM}$. Indeed, as $\Lambda/m_{\rm DM}$ increases, the subleading operators become eventually negligible and the results from the single operators of leading dimension are recovered.

A. Relic density

We use micrOMEGAs code [70] to compute the relic abundance of dark matter in our EFT. We use the single operator hypothesis, and we obtain the coefficients in the Lagrangian—in Eqs. (2) and (3)—such that they reproduce the observed relic density [71]

$$\Omega_{\rm DM}h^2 = 0.1200 \pm 0.0012. \tag{6}$$

In the calculations below, we will use the effective couplings that correctly reproduce the relic density [Eq. (6)].

B. Direct-detection experiments

For the mass range that we are studying, the most stringent limits on spin-independent scattering cross sections of DM and nucleons come from the LUX-ZEPLIN experiment [72]. However, we also include limits from the XENON1T [51] and PandaX-4T [73] experiments. Again we use micrOMEGAs [70] to compute the DM-nucleon cross sections within our EFT, in the limit where the relative velocity goes to zero. Figure 1 shows our results for several operators in our EFT and compares them with the experimental limits. The notation used in this figure is defined in Eq. (4). We can see that OP2, OP5, and the combinations of OP1 and OP2, OP2 and OP3, and OP4 and OP5 are completely ruled out by these experiments. Operators not

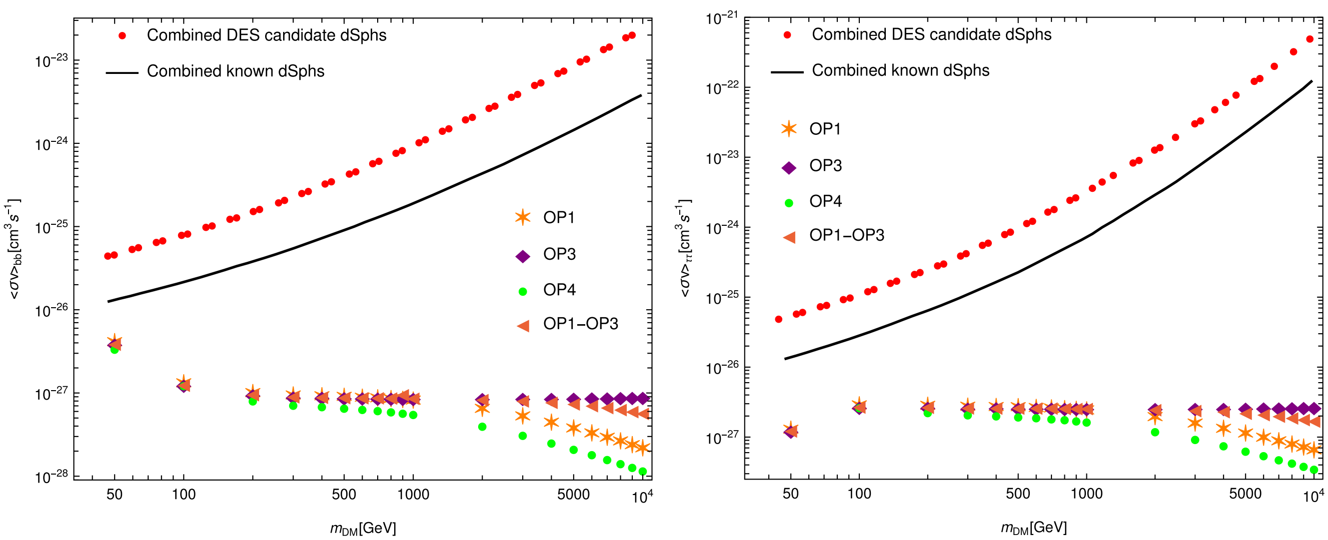

(a) Annihilation into $b\bar{b}$ (b) Annihilation into $\tau^+\tau^-$

FIG. 2. Restrictions from dSphs on the DM annihilation cross sections into (a) $b\bar{b}$ and (b) $\tau^+\tau^-$ for the portals generated by several operators, defined in Eq. (4). We see in both panels that the entire mass region is allowed by the data.

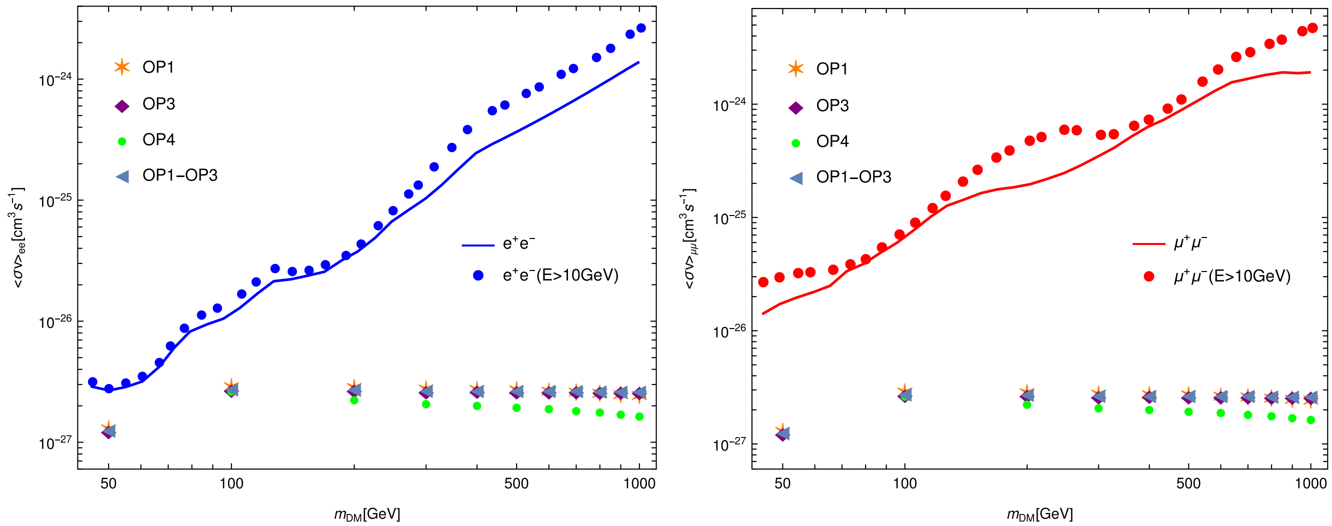

(a) Annihilation into e^+e^- (b) Annihilation into $\mu^+\mu^-$

FIG. 3. Restrictions from AMS-02 data on the DM annihilation cross sections into (a) e^+e^- and (b) $\mu^+\mu^-$ for the portals generated by several operators, defined in Eq. (4). We see that the entire mass region is allowed by the data. The limits shown as solid lines were derived from sampling over various energy windows, while the dashed lines are from considering those windows including only data with energies above 10 GeV [57].

shown in Fig. 1 have DM-nucleon cross sections many orders of magnitude below the current experimental limits from direct-detection experiments. Therefore, in the following we will only consider those operators not plotted in Fig. 1 i.e., OP1, OP3, OP4, and the combination of OP1 and OP3.

C. Dwarf spheroidal satellite galaxies

Using the first year of data from the Dark Energy Survey (DES), eight new dwarf spheroidal satellite galaxies (dSphs) were discovered recently. The dSphs of the Milky Way are some of the most DM-dominated objects known. The dSphs are excellent targets for the indirect detection of DM due to their proximity, high DM content, and apparent absence of nonthermal processes. Analyzing Fermi Large Area Telescope data obtained during six years, Ref. [56] searched for gamma-ray emissions coincident with the positions of these eight new objects. No significant excess of gamma-ray emission was found. Then, in Ref. [56] they computed individual and combined limits on the velocity-averaged DM annihilation cross section for these new targets, assuming that the DES candidates are dSphs with DM halo properties similar to the known dSphs.

Using microOMEGAs [70], we computed the nonrelativistic ($m_{\mathrm{DM}} \ll T$) thermally-averaged DM annihilation cross sections $\langle\sigma v\rangle$, using our effective operators—those that are not ruled out by direct-detection experiments, see Fig. 1—and compared the results with the limits mentioned above. The results are presented in Fig. 2, and we can see that these limits do not help us to constrain our mass region. Note that the combination of operators OP1 and OP3 has a relative sign between its coefficients, because the one with the same sign gives velocity-averaged cross sections even below those shown in the figures.

D. Limits from AMS-02 positron measurements

The AMS-02 Collaboration has presented high-quality measurements of positron fluxes as well as the positron fraction. In Ref. [57] the authors used measurements of the positron flux to derive limits on the dark matter annihilation cross section and lifetime for various final states, and extracted strong limits on DM properties. They worked under the well-motivated assumption that a background positron flux exists from spallations of cosmic rays with the interstellar medium and from astrophysical sources. We again computed the DM annihilation cross sections, now into e^+e^- and $\mu^+\mu^-$, using microOMEGAs [70] and compare them with the bounds derived in Ref. [57]. They also derived limits for the $\tau^+\tau^-$ and $b\bar{b}$ final states, but these are weaker than those from dSphs data. In Fig. 3 we see that our results are below the experimental limits and we cannot rule out any mass region. Note that in this figure we again show the combinations of OP1 and OP3 with a relative sign between their coefficients, while their combination with the same sign gives even smaller values for the velocity-averaged cross sections.

We refine our calculation of the DM annihilation cross sections done previously in Ref. [49][4] and the region of

[4]Before, we used the first two terms of a series expansion of $\langle\sigma v\rangle$ as a function of $x = m/T$, where m stands for the DM mass and T is the temperature. In this work we used microOMEGAs to compute $\langle\sigma v\rangle$ more accurately (the updated values are shown in Fig. 4). This change explains the small difference in the low-mass region of OP4, between the results summarized in Tables I and II.

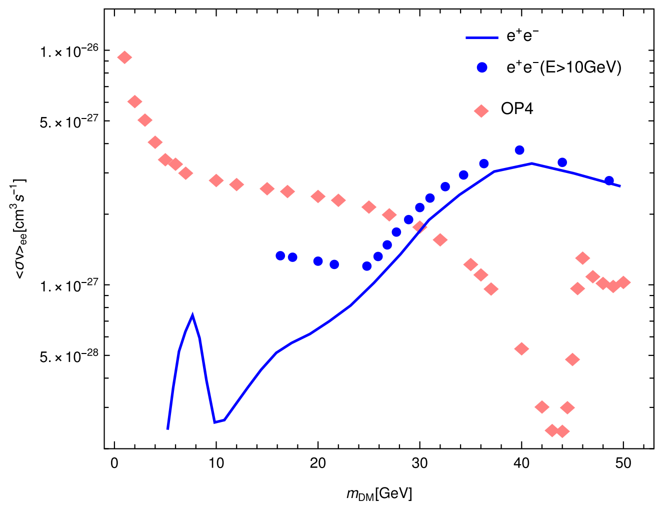

FIG. 4. Restrictions from AMS-02 data on the DM annihilation cross sections into e^+e^- for the portal generated by OP4, defined in Eq. (4). This plot tests the mass region $m_\psi < m_Z/2$, and we see that masses larger than ∼30 GeV are allowed.

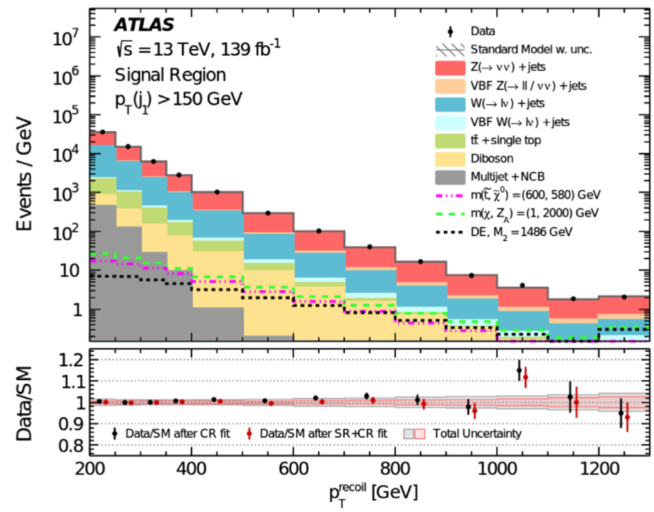

FIG. 5. Measured distributions of p_T^{recoil} for $p_T^{\mathrm{recoil}} > 200$ GeV selection [58] compared with the SM predictions in the signal region.

masses allowed was slightly modified. This change is only noteworthy in the case of the OP4, because the collider constraints exclude masses in the region $m_\psi < m_Z/2$ for OP1, OP3, and the combinations of OP1 and OP3, as we will see below. The data constraining DM annihilation into the final state e^+e^- is the most stringent, therefore it is the one we present here, in Fig. 4. We see that masses smaller than ∼30 GeV are ruled out, while masses in the range [30, 50] GeV are allowed.

E. Is the EFT perturbative?

We want our EFT to be in the perturbative regime, which imposes an upper limit in the dimensionless effective couplings of Eqs. (2) and (3). We bind it using that the corresponding $\alpha = g^2/(4\pi)$, where g^2 stands for any coupling in Eqs. (2) and (3), should be at most ∼1/2 to keep perturbativity. As before, we took the effective couplings that correctly reproduce the relic abundance. We found that, for the OP4 with $m_X \neq m_\Phi$, if the smaller mass is < 1 TeV then the relationships such as $m_X = 3m_\Phi$, and $m_\Phi = 3m_X$ are allowed. While if the smaller mass is 1 TeV $< m <$ 3.2 TeV, the other particle can only be twice as heavy. The quantities that we obtained for the rest of the operators satisfy this criterion of perturbativity.

IV. COLLIDER CONSTRAINTS

The effective operators we are working with allow for the pair production of WIMPs (χ) in the proton-proton collisions at the LHC. If one of the incoming partons radiates a jet through initial-state radiation (ISR), one can observe the process $pp \to \chi\chi j$ as a single jet associated with missing transverse energy ($\not{E}_T$). In this study, we include the ATLAS [58] monojet analysis based on 139 fb^{-1} of data from Run II. ATLAS has performed a number of further searches for other types of ISR, leading for example to monophoton signatures, but these are known to give weaker bounds on DM EFTs than monojet searches [74–76].

Starting from UFO files generated using LanHEP v4.0.0 [77], we have then generated the process $pp \to \chi\chi j$ with MadGraph_aMC@NLO v3.4.0 [78] for the ATLAS analysis, interfaced to PYTHIA v8.3 [79] for parton showering and hadronization. The detector response is simulated using the ATLAS detector configuration [80] in FastJet v3.3.3 [81]. We apply the following kinematic cuts from Ref. [58]: $E_T^{\mathrm{miss}} > 200$ GeV, a leading jet with $p_T > 150$ GeV and $|\eta| < 2.4$, and up to three additional jets with $p_T > 30$ GeV and $|\eta| < 2.8$.

We validated our analysis by reproducing the green dash-dotted line in Fig. 5, using a simplified DM model where Dirac fermion WIMPs (χ) are pair produced from quarks via the s-channel exchange of a spin-one mediator particle (Z_A) with axial-vector couplings [58].

In this analysis we only include the operators (and combinations of them) that still had mass regions with suitable solutions—OP1, OP3, OP4, and the combinations of OP1 and OP2, and OP1 and OP3,—allowed even after all the constraints imposed by noncollider experiments that we have considered. The results reported by ATLAS were obtained using proton-proton collision data at a center-of-mass energy of $\sqrt{s} = 13$ TeV. Events were required to have at least one jet with transverse momentum above 200 GeV and no reconstructed leptons or photons. Due to the $\sqrt{s} = 13$ TeV c.m. energy, the maximum mass we considered in our simulations was 6.4 TeV. We use the data points in Fig. 5 of the measured distributions of p_T^{recoil}.

TABLE I. Summary of results obtained in Ref. [49] considering the Z invisible decay width, relic density, direct-detection experiments and indirect-detection results from dSphs and positron-flux measurements. It is very important to note that we are considering masses of the dark particles below the mass of the Z boson ($M_Z/2$–45.5 GeV, as they appear in charge conjugated pairs).

Operator	Dimension	DM candidate	Allowed DM mass (GeV)
1.- $B_{\mu\nu}\bar{\Psi}\sigma^{\mu\nu}\Psi$	5	Ψ fermion	≈0.0025–2, ≈33–44.5
2.- $(\bar{\psi}\gamma_\mu\psi)(\bar{\Psi}\gamma^\mu P_{L,R}\Psi)$	6	Ψ fermion	none
3.- $B_{\mu\nu}\bar{\Psi}(\gamma^\mu \overleftrightarrow{\mathcal{D}}^\nu - \gamma^\nu \overleftrightarrow{\mathcal{D}}^\mu)P_{L,R}\Psi$	6	Ψ fermion	≈33–44.5
4.- $B_{\mu\nu}X^{\mu\nu}\Phi$	5	vector X, scalar Φ	≈0.11–2, ≈36–44.5
5.- $(\bar{\psi}\gamma_\mu\psi)\frac{1}{2i}\Phi^\dagger \overleftrightarrow{\mathcal{D}}^\mu \Phi$	6	scalar Φ	none
1 ± 2	$5+6$	Ψ fermion	≈0.0025–2
1 ± 3	$5+6$	Ψ fermion	≈0.0025–2, ≈33–44.5
2 ± 3	6	Ψ fermion	none

Renormalization group effects can produce a sizable running of the Wilson coefficients between the low-energy scales probed in direct detection experiments and the high energies of the LHC (see [82–85] and references therein), which depend on $\mathcal{O}_{\rm SM}$, see Eq. (1). For our operators in Eqs. (2) and (3), QCD effects are negligible. We disregarded QED mixing affecting $A_{\rm eff}^{L/R}$ (its corresponding operator, OP2, is excluded in the entire region studied).

V. DISCUSSION AND CONCLUSION

We recall that operators OP2, OP5, and the combinations OP1 + OP2, OP2 + OP3, and OP4 + OP5[5] were already excluded in the range [50 GeV, 6.4 TeV] by direct-detection experiments data. We show below the results obtained by comparing the data from ATLAS [58] (see Fig. 5) with the simulated results for each operator. When we combined operators, for every benchmark point evaluated in the simulations, the relation $\Lambda = 2m_{\rm DM}$ was used.

We also complemented our previous results from Ref. [49],[6] shown in Table I, so we tested the solutions found according to the experimental data analyzed there, in the region $m_{\rm DM} < m_Z/2$. We show below the comparison of the simulated events, for masses previously allowed, with the ATLAS data.

(i) OP1. In Fig. 6 we evaluated $m_\psi = 50$, 100, 200, and 300 GeV and we observe that all these masses are allowed. In Fig. 7 we use the benchmark points (a) 0.0025, 0.01, 0.1, and 2 GeV, and (b) 41, 42, 43, and 44.5 GeV. We see that masses smaller than 43 GeV are ruled out for this operator.

(ii) OP3. We evaluated the masses 175, 190, and 225 GeV in Fig. 8(a) and 35, 40, and 44.5 GeV in Fig. 8(b). We see in Fig. 8(a) that masses larger than 190 GeV are allowed. For this operator the region $m_\psi < M_Z/2$ is now entirely excluded.

(iii) OP4. In Fig. 9 we use the benchmark points: (a) 50, 100, 150, 200, and 300 GeV and (b) 36, 40, and 44.5 GeV. We see in both figures that all values are allowed by the data.

(iv) OP1 and OP2. We use benchmark points for 0.0025, 0.01, 0.1, and 2 GeV in Fig. 10. We see that all these masses are excluded by the data.

(v) OP1 and OP3. We evaluated the masses (a) 200, 300, 325, and 350 GeV, and (b) 50, 100, 140, 150, and 200 GeV. In Fig. 11(a) we use the same sign for the effective couplings and in Fig. 11(b) we use a relative sign between the operators. The masses

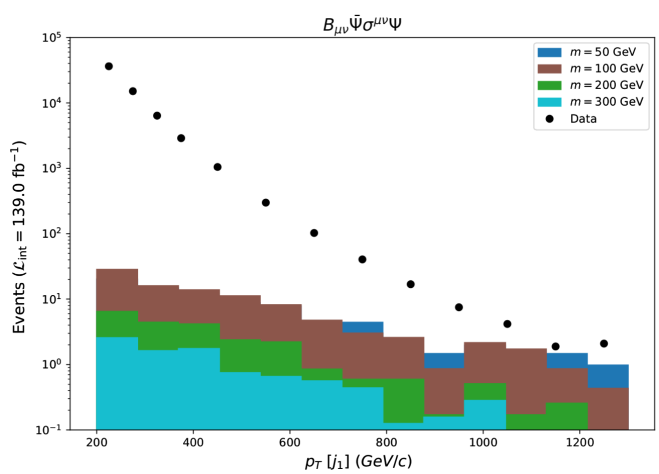

FIG. 6. p_T distributions simulated using OP1 of Eq. (4) vs ATLAS data (Fig. 5). We use benchmark points for 50, 100, 200, and 300 GeV. We see that all these masses are allowed.

[5]The combinations of OP1 and OP2, and OP2 and OP3, are ruled out mainly due to the contribution of OP2 to the spin-independent DM-nucleon cross sections, which does not exclude OP1 or OP3 alone. Similarly, the combination of OP4 and OP5 is excluded mostly due to the contribution of OP5 to the SI DM-nucleon cross sections, which does not exclude OP4 alone.

[6]In Ref. [49] we select benchmark values for Λ (230 GeV < Λ < 1 TeV), but when we combined operators, its value was irrelevant.

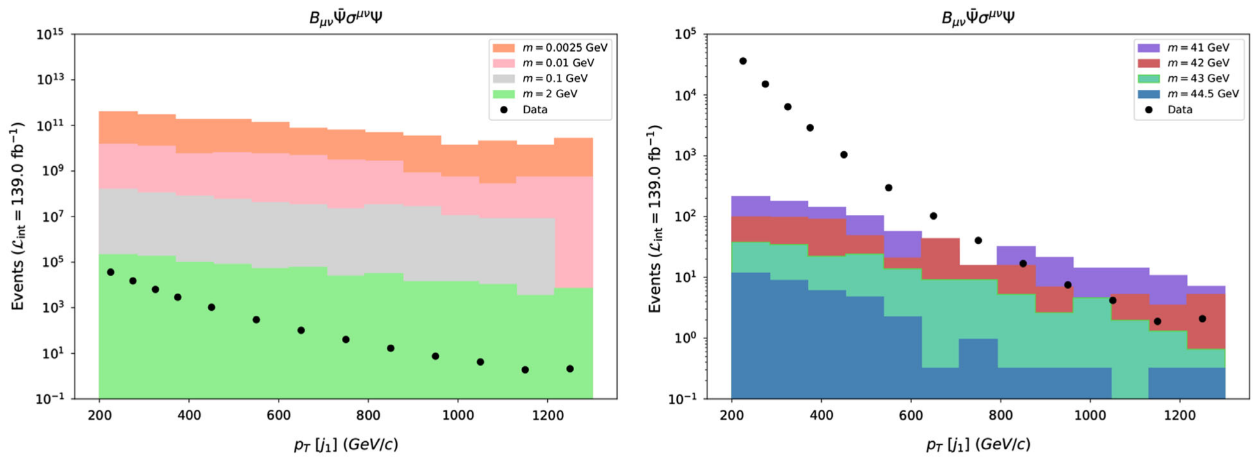

(a) (b)

FIG. 7. p_T distributions simulated using OP1 of Eq. (4) vs ATLAS data (Fig. 5). We use benchmark points for (a) 0.0025, 0.01, 0.1, and 2 GeV, and (b) 41, 42, 43, and 44.5 GeV. We see that masses smaller than 43 GeV are excluded by the data.

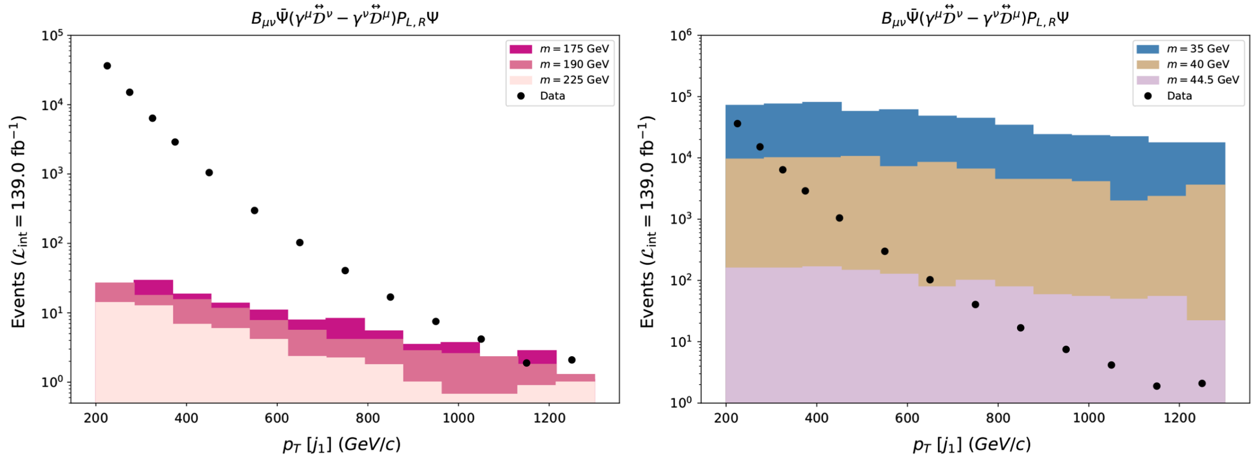

(a) (b)

FIG. 8. p_T distributions simulated using OP3 of Eq. (4), vs ATLAS data (Fig. 5). We use benchmark points for (a) 175, 190, and 225 GeV, and (b) 35, 40, and 44.5 GeV. The plot in (a) shows that masses above 190 GeV are allowed, while in (b) we see that all the region is excluded.

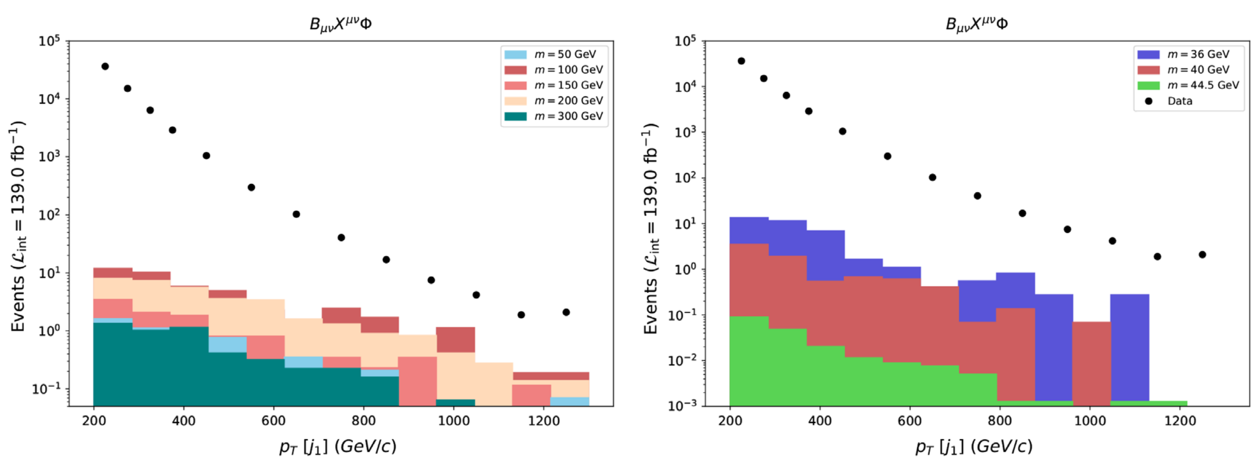

(a) (b)

FIG. 9. p_T distributions simulated using OP4 of Eq. (4), vs ATLAS data (Fig. 5). We use benchmark points for (a) 50, 100, 150, 200, and 300 GeV, and (b) 36, 40, and 44.5 GeV. We see that all these masses are allowed.

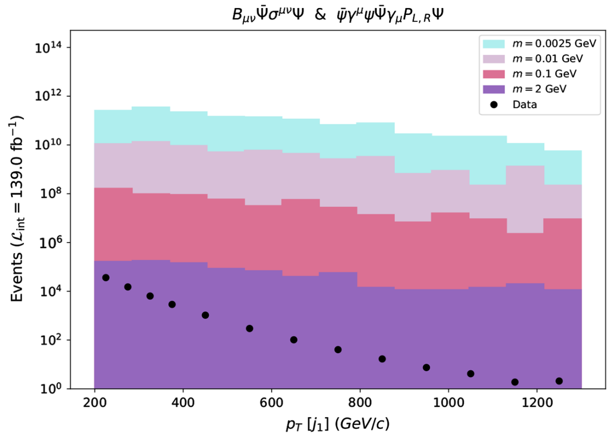

FIG. 10. p_T distributions simulated using OP1 and OP2 of Eq. (4) vs ATLAS data (Fig. 5). We use benchmark points for 0.0025, 0.01, 0.1, and 2 GeV. We see that all these masses are ruled out.

allowed are (a) larger than 325 GeV, and (b) larger than 140 GeV. Finally, for DM masses below $M_Z/2$, we tested the benchmark points: Fig. 12(a) 0.0025, 0.01, 0.1, and 2 GeV and Fig. 12(b) 35, 40, and 44 GeV. We see that in both figures the whole mass range is ruled out by the data ($m_{\rm DM} \in [44\ \text{GeV}, M_Z/2]$ was already excluded by analysis of positron measurements, see Table I).

We present a summary of our results in Table II.

The constraining power of ATLAS results forbids mostly light DM particles with masses below $M_Z/2$. For OP1 and OP4, we still have solutions below $M_Z/2$, while for OP3 and the combination of OP1 and OP3 we need larger masses to satisfy the ATLAS constraints. Future LHC analyses will set even tighter constraints on DM, particularly within our EFT and, specifically, for the subset of

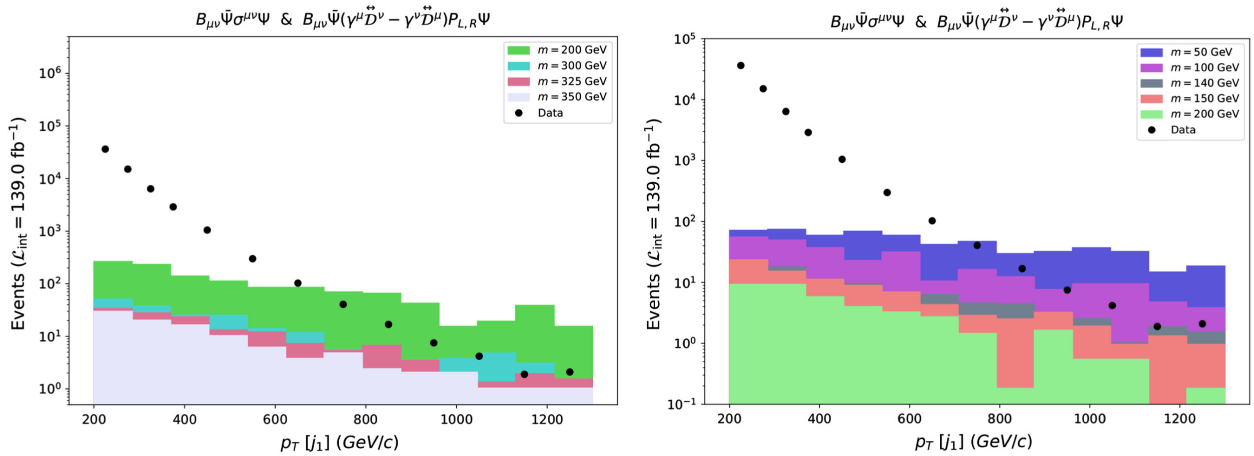

(a) OP1+OP3 (b) OP1-OP3

FIG. 11. p_T distributions simulated using (a) OP1 + OP3 and (b) OP1–OP3 of Eq. (4), vs ATLAS data (Fig. 5). We use benchmark points for (a) 200, 300, 325, and 350 GeV, and (b) 50, 100, 140, 150, and 200 GeV. The masses allowed are (a) above 325 GeV and (b) above 140 GeV.

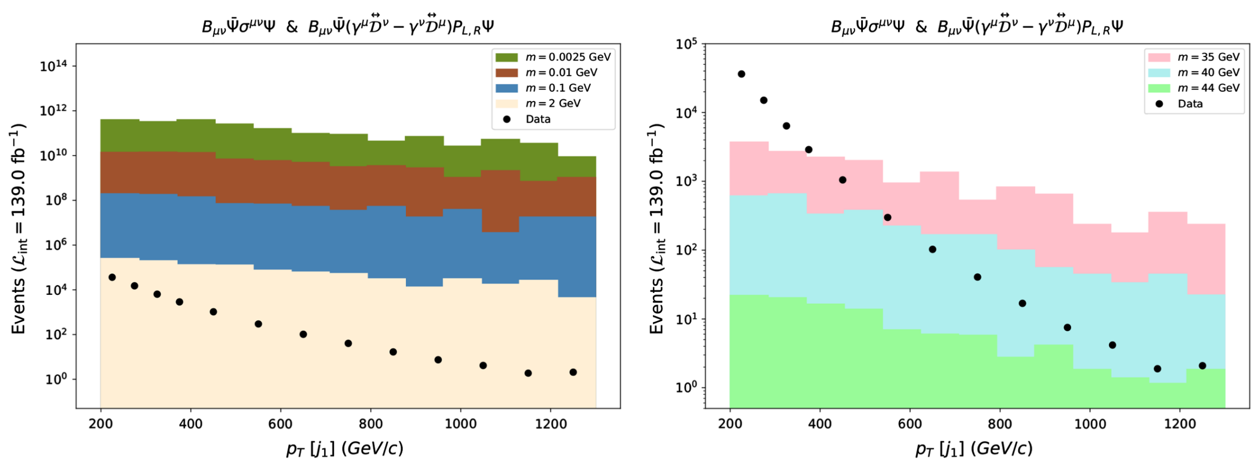

(a) (b)

FIG. 12. p_T distributions simulated using OP1 and OP3 of Eq. (4) vs ATLAS data (Fig. 5). We use benchmark points for (a) 0.0025, 0.01, 0.1, and 2 GeV, and (b) 35, 40, and 44 GeV. In (a) all the masses are ruled out by the data, while in (b) masses larger than 44 GeV are allowed.

TABLE II. Summary of results obtained in this work, which supersede those in our previous paper [49]. In addition to the experimental constraints used therein, now we also considered the limits from ATLAS in Ref. [58].

Operator	Dimension	DM candidate	Allowed DM mass
1.- $B_{\mu\nu}\bar{\Psi}\sigma^{\mu\nu}\Psi$	5	Ψ fermion	$\gtrsim$43 GeV[a]
2.- $(\bar{\psi}\gamma_\mu\psi)(\bar{\Psi}\gamma^\mu P_{L,R}\Psi)$	6	Ψ fermion	none
3.- $B_{\mu\nu}\bar{\Psi}(\gamma^\mu \overleftrightarrow{\mathcal{D}}^\nu - \gamma^\nu \overleftrightarrow{\mathcal{D}}^\mu)P_{L,R}\Psi$	6	Ψ fermion	$\gtrsim$190 GeV
4.- $B_{\mu\nu}X^{\mu\nu}\Phi$	5	vector X, scalar Φ	$\gtrsim$30 GeV[a]
5.- $(\bar{\psi}\gamma_\mu\psi)\frac{1}{2i}\Phi^\dagger \overleftrightarrow{\mathcal{D}}^\mu \Phi$	6	scalar Φ	none
1 ± 2	$5+6$	Ψ fermion	none
$1+3$	$5+6$	Ψ fermion	$\gtrsim$325 GeV
$1-3$	$5+6$	Ψ fermion	$\gtrsim$140 GeV
2 ± 3	6	Ψ fermion	none

[a]We note that the region $(M_Z \pm \Gamma_Z)/2$ is excluded, see Table I.

operators (those with spin-one mediators) considered in this work.

ACKNOWLEDGMENTS

We are grateful to José Wudka for valuable discussions and suggestions and to Marco A. Arroyo-Ureña for his helpful guide and advice with the software used in this work. We also thank the anonymous referee for a particularly helpful review. F. F. acknowledges financial support from CONACyT graduate Grants Program No. 728500. P. R is indebted to Cátedras Marcos Moshinsky (Fundación Marcos Moshinsky) and CONACyT (“Paradigmas y Controversias de la Ciencia 2022,” Project No. 319395).

[1] G. Arcadi, M. Dutra, P. Ghosh, M. Lindner, Y. Mambrini, M. Pierre, S. Profumo, and F. S. Queiroz, The waning of the wimp? A review of models, searches, and constraints, Eur. Phys. J. C **78**, 203 (2018).
[2] Leszek Roszkowski, Enrico Maria Sessolo, and Sebastian Trojanowski, WIMP dark matter candidates and searches—current status and future prospects, Rep. Prog. Phys. **81**, 066201 (2018).
[3] Marc Schumann, Direct detection of WIMP dark matter: Concepts and status, J. Phys. G **46**, 103003 (2019).
[4] Changbo Fu *et al.*, Spin-Dependent Weakly-Interacting-Massive-Particle–Nucleon Cross Section Limits from First Data of PandaX-II Experiment, Phys. Rev. Lett. **118**, 071301 (2017); Changbo Fu, Phys. Rev. Lett. **120**, 049902(E) (2018).
[5] E. Aprile *et al.*, First Dark Matter Search Results from the XENON1T Experiment, Phys. Rev. Lett. **119**, 181301 (2017).
[6] D. S. Akerib *et al.*, Results on the Spin-Dependent Scattering of Weakly Interacting Massive Particles on Nucleons from the Run 3 Data of the LUX Experiment, Phys. Rev. Lett. **116**, 161302 (2016).
[7] E. Behnke *et al.*, Final results of the PICASSO dark matter search experiment, Astropart. Phys. **90**, 85 (2017).
[8] D. S. Akerib *et al.*, Results from a Search for Dark Matter in the Complete LUX Exposure, Phys. Rev. Lett. **118**, 021303 (2017).
[9] Andi Tan *et al.*, Dark Matter Results from First 98.7 Days of Data from the PandaX-II Experiment, Phys. Rev. Lett. **117**, 121303 (2016).
[10] Shaul Hanany *et al.*, PICO: Probe of Inflation and Cosmic Origins, arXiv:1902.10541.
[11] Dan Hooper and Lisa Goodenough, Dark matter annihilation in the Galactic Center as seen by the Fermi Gamma Ray Space Telescope, Phys. Lett. B **697**, 412 (2011).
[12] Esra Bulbul, Maxim Markevitch, Adam Foster, Randall K. Smith, Michael Loewenstein, and Scott W. Randall, Detection of an unidentified emission line in the stacked x-ray spectrum of galaxy clusters, Astrophys. J. **789**, 13 (2014).
[13] O. Urban, N. Werner, S. W. Allen, A. Simionescu, J. S. Kaastra, and L. E. Strigari, A Suzaku search for dark matter emission lines in the X-ray brightest galaxy clusters, Mon. Not. R. Astron. Soc. **451**, 2447 (2015).
[14] K. Choi *et al.*, Search for Neutrinos from Annihilation of Captured Low-Mass Dark Matter Particles in the Sun by Super-Kamiokande, Phys. Rev. Lett. **114**, 141301 (2015).
[15] Oleg Ruchayskiy, Alexey Boyarsky, Dmytro Iakubovskyi, Esra Bulbul, Dominique Eckert, Jeroen Franse, Denys Malyshev, Maxim Markevitch, and Andrii Neronov, Searching for decaying dark matter in deep XMM–Newton observation of the Draco dwarf spheroidal, Mon. Not. R. Astron. Soc. **460**, 1390 (2016).
[16] M. Ackermann *et al.*, Searching for Dark Matter Annihilation from Milky Way Dwarf Spheroidal Galaxies with Six Years of Fermi Large Area Telescope Data, Phys. Rev. Lett. **115**, 231301 (2015).

[17] Jeroen Franse *et al.*, Radial profile of the 3.55 keV line out to R_{200} in the perseus cluster, Astrophys. J. **829**, 124 (2016).

[18] F. A. Aharonian *et al.*, *Hitomi* constraints on the 3.5 keV line in the Perseus galaxy cluster, Astrophys. J. **837**, L15 (2017).

[19] Ming-Yang Cui, Qiang Yuan, Yue-Lin Sming Tsai, and Yi-Zhong Fan, Possible Dark Matter Annihilation Signal in the AMS-02 Antiproton Data, Phys. Rev. Lett. **118**, 191101 (2017).

[20] M. G. Aartsen *et al.*, Search for annihilating dark matter in the Sun with 3 years of IceCube data, Eur. Phys. J. C **77**, 146 (2017); **79**, 214(E) (2019).

[21] M. Ackermann *et al.*, The fermi galactic center GeV excess and implications for dark matter, Astrophys. J. **840**, 43 (2017).

[22] N. Aghanim *et al.*, Planck 2018 results. VI. Cosmological parameters, Astron. Astrophys. **641**, A6 (2020); **652**, C4(E) (2021).

[23] G. Belanger, F. Boudjema, A. Pukhov, and A. Semenov, Dark matter direct detection rate in a generic model with micrOMEGAs 2.2, Comput. Phys. Commun. **180**, 747 (2009).

[24] Jessica Goodman, Masahiro Ibe, Arvind Rajaraman, William Shepherd, Tim M. P. Tait, and Hai-Bo Yu, Constraints on dark matter from colliders, Phys. Rev. D **82**, 116010 (2010).

[25] Andreas Crivellin and Ulrich Haisch, Dark matter direct detection constraints from gauge bosons loops, Phys. Rev. D **90**, 115011 (2014).

[26] Andreas Crivellin, Francesco D'Eramo, and Massimiliano Procura, New Constraints on Dark Matter Effective Theories from Standard Model Loops, Phys. Rev. Lett. **112**, 191304 (2014).

[27] Mateusz Duch, Bohdan Grzadkowski, and Jose Wudka, Classification of effective operators for interactions between the standard model and dark matter, J. High Energy Phys. 05 (2015) 116.

[28] Subhaditya Bhattacharya and Jose Wudka, Effective theories with dark matter applications, Int. J. Mod. Phys. D **30**, 2130004 (2021).

[29] Basabendu Barman, Subhaditya Bhattacharya, Sudhakantha Girmohanta, and Sahabub Jahedi, Effective leptophilic WIMPs at the e^+e^- collider, J. High Energy Phys. 04 (2022) 146.

[30] Giorgio Arcadi, Abdelhak Djouadi, and Martti Raidal, Dark Matter through the Higgs portal, Phys. Rep. **842** , 1 (2020).

[31] Nicolas Cosme, Laura Lopez Honorez, and Michel H. G. Tytgat, Leptogenesis and dark matter related?, Phys. Rev. D **72**, 043505 (2005).

[32] Haipeng An, Shao-Long Chen, Rabindra N. Mohapatra, and Yue Zhang, Leptogenesis as a common origin for matter and dark matter, J. High Energy Phys. 03 (2010) 124.

[33] Adam Falkowski, Jose Juknevich, and Jessie Shelton, Dark matter through the neutrino portal, arXiv:0908.1790.

[34] Manfred Lindner, Alexander Merle, and Viviana Niro, Enhancing dark matter annihilation into neutrinos, Phys. Rev. D **82**, 123529 (2010).

[35] Yasaman Farzan, Flavoring monochromatic neutrino flux from dark matter annihilation, J. High Energy Phys. 02 (2012) 091.

[36] Adam Falkowski, Joshua T. Ruderman, and Tomer Volansky, Asymmetric dark matter from leptogenesis, J. High Energy Phys. 05 (2011) 106.

[37] Julian Heeck and He Zhang, Exotic charges, multicomponent dark matter and light sterile neutrinos, J. High Energy Phys. 05 (2013) 164.

[38] Seungwon Baek, P. Ko, and Wan-Il Park, Singlet portal extensions of the standard seesaw models to a dark sector with local dark symmetry, J. High Energy Phys. 07 (2013) 013.

[39] Iason Baldes, Nicole F. Bell, Alexander J. Millar, and Raymond R. Volkas, Asymmetric dark matter and *CP* violating scatterings in a UV complete model, J. Cosmol. Astropart. Phys. 10 (2015) 048.

[40] Vannia González-Macías, José I. Illana, and José Wudka, A realistic model for dark matter interactions in the neutrino portal paradigm, J. High Energy Phys. 05 (2016) 171.

[41] Brian Batell, Tao Han, and Barmak Shams Es Haghi, Indirect detection of neutrino portal dark matter, Phys. Rev. D **97**, 095020 (2018).

[42] S. HajiSadeghi, S. Smolenski, and J. Wudka, Asymmetric dark matter with a possible Bose-Einstein condensate, Phys. Rev. D **99**, 023514 (2019).

[43] Priyotosh Bandyopadhyay, Eung Jin Chun, Rusa Mandal, and Farinaldo S. Queiroz, Scrutinizing right-handed neutrino portal dark matter with Yukawa effect, Phys. Lett. B **788**, 530 (2019).

[44] Asher Berlin and Nikita Blinov, Thermal neutrino portal to sub-MeV dark matter, Phys. Rev. D **99**, 095030 (2019).

[45] M. Blennow, E. Fernandez-Martinez, A. Olivares-Del Campo, S. Pascoli, S. Rosauro-Alcaraz, and A. V. Titov, Neutrino portals to dark matter, Eur. Phys. J. C **79**, 555 (2019).

[46] Eleanor Hall, Thomas Konstandin, Robert McGehee, and Hitoshi Murayama, Asymmetric matters from a dark first-order phase transition, Phys. Rev. D **107**, 055011 (2023).

[47] Eleanor Hall, Thomas Konstandin, Robert McGehee, Hitoshi Murayama, and Géraldine Servant, Baryogenesis from a dark first-order phase transition, J. High Energy Phys. 04 (2020) 042.

[48] Vannia Gonzalez Macias and Jose Wudka, Effective theories for Dark Matter interactions and the neutrino portal paradigm, J. High Energy Phys. 07 (2015) 161.

[49] Fabiola Fortuna, Pablo Roig, and José Wudka, Effective field theory analysis of dark matter-standard model interactions with spin one mediators, J. High Energy Phys. 02 (2021) 223.

[50] R. L. Workman *et al.*, Review of particle physics, Prog. Theor. Exp. Phys. **2022**, 083C01 (2022).

[51] E. Aprile *et al.*, Dark Matter Search Results from a One Ton-Year Exposure of XENON1T, Phys. Rev. Lett. **121**, 111302 (2018).

[52] Xiangxiang Ren *et al.*, Constraining Dark Matter Models with a Light Mediator at the PandaX-II Experiment, Phys. Rev. Lett. **121**, 021304 (2018).

[53] D. S. Akerib *et al.*, Results of a Search for Sub-GeV Dark Matter Using 2013 LUX Data, Phys. Rev. Lett. **122**, 131301 (2019).

[54] P. Agnes *et al.*, Constraints on Sub-GeV Dark-Matter–Electron Scattering from the DarkSide-50 Experiment, Phys. Rev. Lett. **121**, 111303 (2018).

[55] A. H. Abdelhameed *et al.*, First results from the CRESST-III low-mass dark matter program, Phys. Rev. D **100**, 102002 (2019).

[56] A. Drlica-Wagner *et al.*, Search for gamma-ray emission from DES dwarf spheroidal galaxy candidates with Fermi-LAT data, Astrophys. J. **809**, L4 (2015).

[57] Alejandro Ibarra, Anna S. Lamperstorfer, and Joseph Silk, Dark matter annihilations and decays after the AMS-02 positron measurements, Phys. Rev. D **89**, 063539 (2014).

[58] Georges Aad *et al.*, Search for new phenomena in events with an energetic jet and missing transverse momentum in pp collisions at $\sqrt{s} = 13$ TeV with the ATLAS detector, Phys. Rev. D **103**, 112006 (2021).

[59] Davide Racco, Andrea Wulzer, and Fabio Zwirner, Robust collider limits on heavy-mediator Dark Matter, J. High Energy Phys. 05 (2015) 009.

[60] Nicole F. Bell, Yi Cai, James B. Dent, Rebecca K. Leane, and Thomas J. Weiler, Dark matter at the LHC: Effective field theories and gauge invariance, Phys. Rev. D **92**, 053008 (2015).

[61] Andrea De Simone and Thomas Jacques, Simplified models vs. effective field theory approaches in dark matter searches, Eur. Phys. J. C **76**, 367 (2016).

[62] Qing-Hong Cao, Chuan-Ren Chen, Chong Sheng Li, and Hao Zhang, Effective dark matter model: Relic density, CDMS II, Fermi LAT and LHC, J. High Energy Phys. 08 (2011) 018.

[63] Kingman Cheung, Po-Yan Tseng, Yue-Lin S. Tsai, and Tzu-Chiang Yuan, Global constraints on effective dark matter interactions: Relic density, direct detection, indirect detection, and collider, J. Cosmol. Astropart. Phys. 05 (2012) 001.

[64] Giorgio Busoni, Andrea De Simone, Enrico Morgante, and Antonio Riotto, On the validity of the effective field theory for dark matter searches at the LHC, Phys. Lett. B **728**, 412 (2014).

[65] Oliver Buchmueller, Matthew J. Dolan, Sarah A. Malik, and Christopher McCabe, Characterising dark matter searches at colliders and direct detection experiments: Vector mediators, J. High Energy Phys. 01 (2015) 037.

[66] Brian Patt and Frank Wilczek, Higgs-field portal into hidden sectors, arXiv:hep-ph/0605188.

[67] J. M. Lamprea, E. Peinado, S. Smolenski, and J. Wudka, Strongly interacting neutrino portal dark matter, Phys. Rev. D **103**, 015017 (2021).

[68] Basabendu Barman, Subhaditya Bhattacharya, and Bohdan Grzadkowski, Feebly coupled vector boson dark matter in effective theory, J. High Energy Phys. 12 (2020) 162.

[69] Peter Athron *et al.*, Thermal WIMPs and the scale of new physics: Global fits of Dirac dark matter effective field theories, Eur. Phys. J. C **81**, 992 (2021).

[70] G. Bélanger, F. Boudjema, A. Pukhov, and A. Semenov, micrOMEGAs4.1: Two dark matter candidates, Comput. Phys. Commun. **192**, 322 (2015).

[71] P. A. Zyla *et al.*, Review of particle physics, Prog. Theor. Exp. Phys. **2020**, 083C01 (2020).

[72] J. Aalbers *et al.*, First dark matter search results from the LUX-ZEPLIN (LZ) experiment, arXiv:2207.03764.

[73] Yue Meng *et al.*, Dark Matter Search Results from the PandaX-4T Commissioning Run, Phys. Rev. Lett. **127**, 261802 (2021).

[74] Ning Zhou, David Berge, and Daniel Whiteson, Mono-everything: Combined limits on dark matter production at colliders from multiple final states, Phys. Rev. D **87**, 095013 (2013).

[75] A. J. Brennan, M. F. McDonald, J. Gramling, and T. D. Jacques, Collide and conquer: Constraints on simplified dark matter models using mono-X collider searches, J. High Energy Phys. 05 (2016) 112.

[76] Martin Bauer, Martin Klassen, and Valentin Tenorth, Universal properties of pseudoscalar mediators in dark matter extensions of 2HDMs, J. High Energy Phys. 07 (2018) 107.

[77] A. Semenov, LanHEP—A package for automatic generation of Feynman rules from the Lagrangian. Version 3.2, Comput. Phys. Commun. **201**, 167 (2016).

[78] J. Alwall, R. Frederix, S. Frixione, V. Hirschi, F. Maltoni, O. Mattelaer, H. S. Shao, T. Stelzer, P. Torrielli, and M. Zaro, The automated computation of tree-level and next-to-leading order differential cross sections, and their matching to parton shower simulations, J. High Energy Phys. 07 (2014) 079.

[79] Christian Bierlich *et al.*, A comprehensive guide to the physics and usage of PYTHIA 8.3, SciPost Phys. Codebases **8**, (2022).

[80] Jack Y. Araz, Benjamin Fuks, and Georgios Polykratis, Simplified fast detector simulation in MadAnalysis 5, Eur. Phys. J. C **81**, 329 (2021).

[81] Matteo Cacciari, Gavin P. Salam, and Gregory Soyez, FastJet user manual, Eur. Phys. J. C **72**, 1896 (2012).

[82] Fady Bishara, Joachim Brod, Benjamin Grinstein, and Jure Zupan, Chiral effective theory of dark matter direct detection, J. Cosmol. Astropart. Phys. 02 (2017) 009.

[83] Fady Bishara, Joachim Brod, Benjamin Grinstein, and Jure Zupan, DirectDM: A tool for dark matter direct detection, arXiv:1708.02678.

[84] Fady Bishara, Joachim Brod, Benjamin Grinstein, and Jure Zupan, From quarks to nucleons in dark matter direct detection, J. High Energy Phys. 11 (2017) 059.

[85] Fady Bishara, Joachim Brod, Benjamin Grinstein, and Jure Zupan, Renormalization group effects in dark matter interactions, J. High Energy Phys. 03 (2020) 089.